

Article

Prototyping of an All-pMOS-Based Cross-Coupled Voltage Multiplier in Single-Well CMOS Technology for Energy Harvesting Utilizing a Gastric Acid Battery

Shinya Yoshida ^{1,*} , Hiroshi Miyaguchi ² and Tsutomu Nakamura ³¹ Graduate School of Engineering, Tohoku University, Sendai 980-8579, Japan² Micro System Integration Center, Tohoku University, Sendai 980-8579, Japan³ Promotion Office of Strategic Innovation, Tohoku University, Sendai 980-8579, Japan

* Correspondence: s-yoshida@mems.mech.tohoku.ac.jp; Tel.: +81-22-752-2192

Received: 1 June 2019; Accepted: 13 July 2019; Published: 18 July 2019



Abstract: A gastric acid battery and its charge storage in a capacitor are a simple and safe method to provide a power source to an ingestible device. For that method, the electromotive force of the battery should be boosted for storing a large amount of energy. In this study, we have proposed an all-p-channel metal-oxide semiconductor (pMOS)-based cross-coupled voltage multiplier (CCVM) utilizing single-well CMOS technology to achieve a voltage boosting higher than from a conventional complementary MOS (CMOS) CCVM. We prototyped a custom integrated circuit (IC) implemented with the above CCVMs and a ring oscillator as a clock source. The characterization experiment demonstrated that our proposed pMOS-based CCVM can boost the input voltage higher because it avoids the body effect problem resulting from an n-channel MOS transistor. This circuit was also demonstrated to significantly reduce the circuit area on the IC, which is advantageous as it reduces the chip size or provides an area for other functional circuits. This simple circuit structure based on mature and low-cost technologies matches well with disposal applications such as an ingestible device. We believe that this pMOS-based CCVM has the potential to become a useful energy harvesting circuit for ingestible devices.

Keywords: ingestible device; gastric acid battery; cross-coupled voltage multiplier; charge pump; body effect

1. Introduction

An ingestible device has been developed as an ideal device for diagnosis and healthcare for use in the near future [1–3]. Various ingestible devices implemented with temperature [4,5], pH [6], and gas [7] sensors have been released or developed thus far. However, most devices generally use a button battery as the power source. This has a significant risk of accidentally injuring the inside of the body, and thus, has been one of the barriers for such ingestible devices to be widely supplied for consumer applications. Its lifetime and expiry are also inconvenient factors. Recently, a wireless power supply based on induction from outside of the body was proposed [8]. However, the ingestible device remains at a deep position in the body and moves along the gastrointestinal tract. Therefore, it is difficult to efficiently supply power to the device. The exposure dose amount of the body might be increased if the fed power is increased for forcibly providing a rapid energy charge.

Recently, a gastric acid battery using galvanic couples has received considerable attention as a safe power source for ingestible devices. However, a drawback is that the power is basically generated only in the stomach while the battery electrode survives. The generated power decreases significantly in the intestinal fluids even if galvanic electrodes operable in the intestine are employed [9]. Moreover, the

generated power might become unstable in the intestine owing to the contamination of the electrode surface by stool. This feature of the gastric acid battery significantly limits its applications, although it is apparently suitable for medication management devices which are intended to operate only in the stomach [10,11].

Therefore, we have proposed to store the generated energy in a storage medium such as a multi-layer ceramic capacitor (MLCC) for device operation even in the intestines, as shown in Figure 1 [12,13]. First, in the energy harvesting domain, the power generated by the gastric acid battery operates an oscillator and a voltage-boosting circuit. Then, the generated energy is stored in the capacitor at a boosted voltage permitted by the hardware specifications while the device remains in the stomach. In the sensing, processing, and communication domain, the stored energy is distributed to other components such as the sensor, processing circuit, and driver circuit for telecommunication. This method allows device operation until the voltage of the storage capacitor falls below the operable voltage of the electrical components. Following this principle, and unlike a typical battery, a voltage regulator, which is associated with power loss, is not needed. A short time charge is also expected. Using this method, we tune the number of voltage-boosting stages to store greater energy in the MLCC, but not to exceed the hardware specifications.

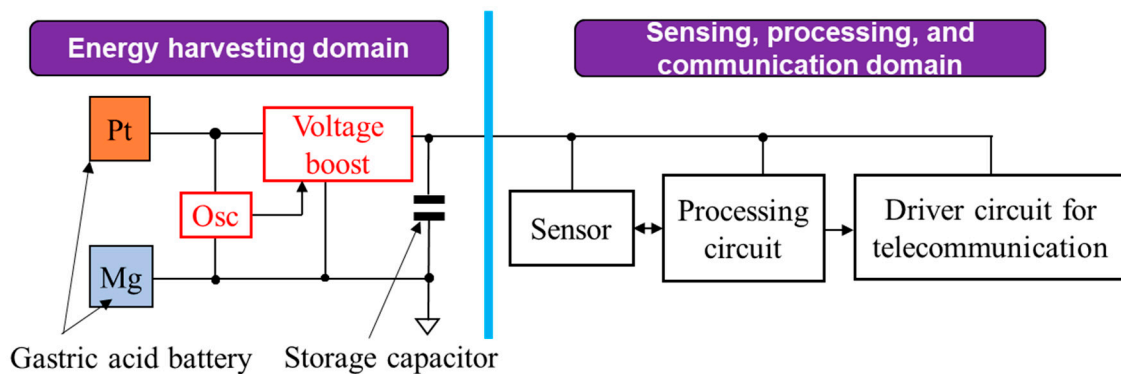


Figure 1. Schematic of an ingestible sensor system based on a stored charge as a power source utilizing a gastric acid battery via a voltage-boosting circuit.

In our previous study, a conventional complementary metal-oxide semiconductor (CMOS)-based cross-coupled voltage multiplier (CCVM) was used for the voltage boosting of a gastric acid battery [12,13]. Figure 2a shows one stage of the CCVM. V_{gen} corresponds to the output voltage generated by the gastric acid battery. CLK_1 and CLK_2 are two-phase clocks and have amplitudes of V_{gen} . These clocks are symmetrically connected to pumping capacitors and pump V_{gen} up alternatively. We prototyped a four-stage cascaded CCVM and successfully demonstrated that it boosted the output of the gastric acid battery.

However, for the above-mentioned CCVM, the boosting performance gradually decreases with the number of stages [14,15]. This is caused by the body effect of the n-channel MOS (nMOS) transistor. One approach to compensate the degradation in the boosting performance is to increase the transistor size or parallel number in the latter stages. However, this approach increases the occupied area of the CCVM in an integrated circuit (IC), which will limit the usable areas for other circuits or enlarge the chip size. Another method is to use a special process such as a double-well structure or a silicon on insulator (SOI) process for separating the p-well in each stage. However, the fabrication process cost increases significantly. An IC cost should be inexpensive for such a disposal device.

Consequently, p-channel MOS (pMOS)-based charge pumps were proposed for eliminating this body effect problem of an nMOS transistor. For example, a charge pump with four-phase clocks is reported to exhibit a highly efficient voltage boosting [16–18]. However, such a multiple-clock-based charge pump requires a circuit with a complex design. By contrast, charge pumps utilizing twin- or triple-well CMOS technologies have been reported [19–21]. However, these multiple-well technologies

are generally more expensive than a single-well CMOS technology. A low cost is more important than efficiency for a disposal ingestible device.

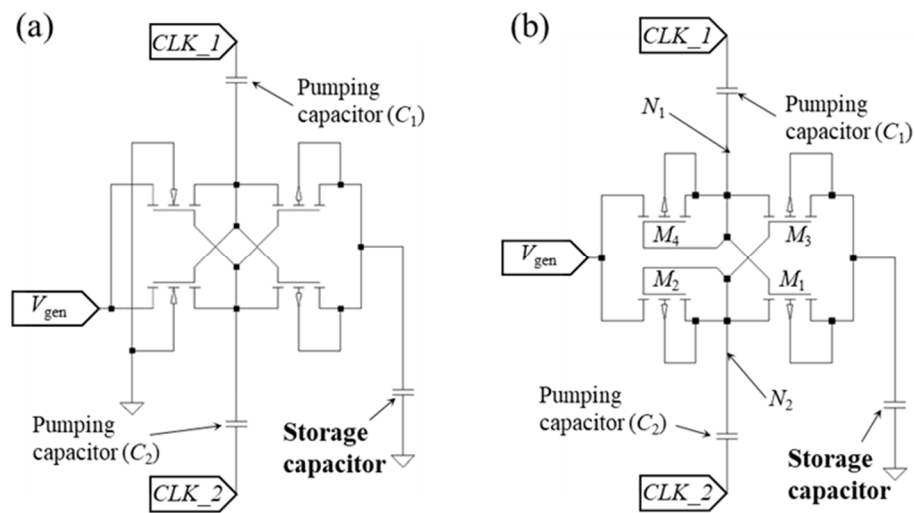


Figure 2. Schematic of (a) a conventional CMOS-based CCVM and (b) an all-p-channel metal-oxide semiconductor (pMOS)-based CCVM.

Therefore, we have proposed a pMOS-based CCVM operated by two-phase clocks in a single-well CMOS technology, which is assumed in this study to be utilized for an ingestible device application. We prototyped this pMOS-based CCVM and a conventional one in the same IC die and compared their voltage-boosting performances. A two-phase-clock generator based on an oscillating circuit was also fabricated and characterized. Finally, we demonstrated the operation of these circuits and the boosting of the electromotive force of a pair of Mg and Pt electrodes acting as a gastric acid battery by dipping them in an artificial gastric juice.

2. Fabrication of the CCVM Circuits in a Custom IC

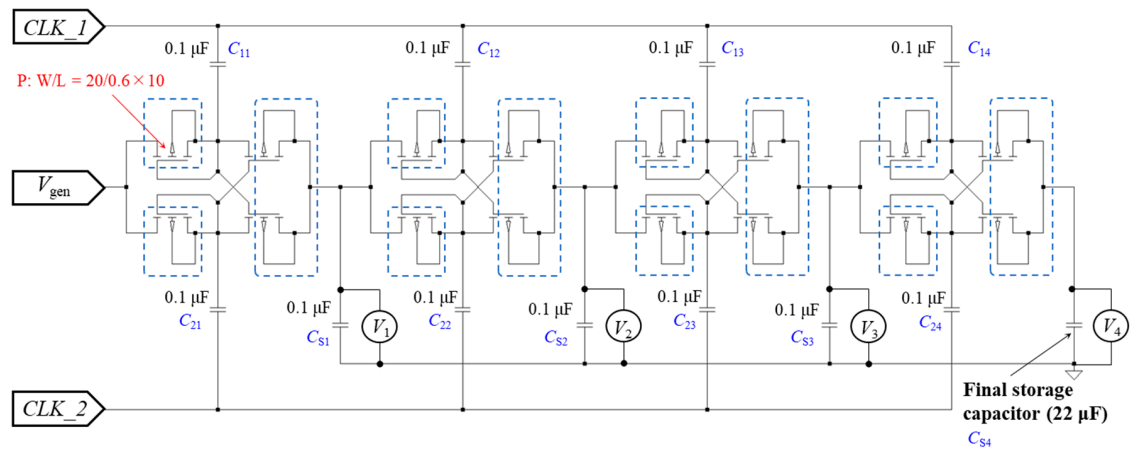
Figure 2b shows the schematic of a single stage of the pMOS-based CCVM. Here, M_1 and M_2 as the pMOS transistors are focused on to easily explain the boosting procedure. During the first half cycle, CLK_1 changes from 0 to V_{gen} and CLK_2 changes from V_{gen} to 0, and then, M_1 and M_2 turn OFF and ON, respectively. Thus, the coupling capacitor, C_2 , is charged by V_{gen} via the M_2 and N_2 nodes. Next, in the second half cycle, when CLK_1 and CLK_2 respectively change to 0 and V_{gen} , M_1 and M_2 turn ON and OFF, respectively. At this instant, node N_2 is ideally boosted to $2 \times V_{gen}$ by the coupling of C_2 . Therefore, the storage capacitor is charged at the boosted voltage. A similar circuit composed of M_3 , M_4 , and N_1 nodes is fabricated and driven by the same CLK_1 and CLK_2 but in a reversed phase for dual-phase charge pumping. The voltage can be boosted up further by cascading the stages. The ideal output voltage of a circuit with n stages is shown as follows:

$$V_{out} = V_{gen} + n \times V_{gen}. \quad (1)$$

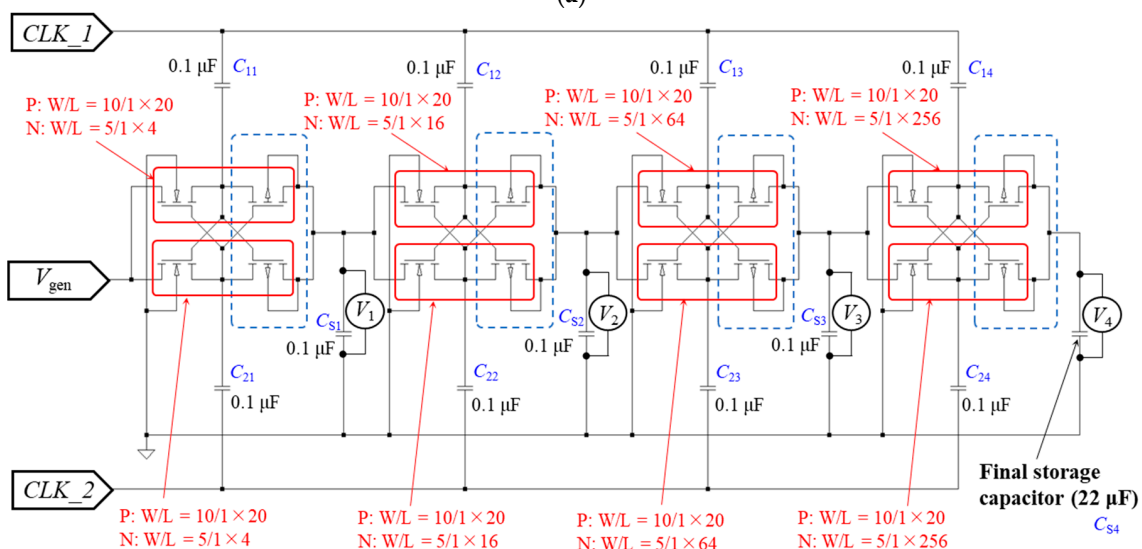
In practice, V_{out} is decreased by certain factors such as the parasitic stray capacitance at each pumping node, undesired leakage current, time constant, and threshold voltage of the transistors.

Figure 3a shows the circuit schematic of the pMOS-based CCVM as designed and prototyped in this study. In this figure, the expression “P: W/L = 20/0.6 × 10” implies that 10 pMOS transistors with a gate width and length of 20 and 0.6 μm , respectively, are connected in parallel. The N-wells of the transistors, which are surrounded by the dashed blue lines, are separated for applying a different potential to each transistor. MLCCs of 0.1 μF (C_{11} , C_{12} , C_{13} , C_{14} , C_{21} , C_{22} , C_{23} , C_{24}) are used as the coupling capacitors. The charge is stored in the intermediate storage capacitors (C_{S1} , C_{S2} , C_{S3}) of 0.1 μF

MLCC at the intermediate boosted voltage at each stage and eventually in the final storage capacitor (C_{S4}). A 22 μF electrolytic capacitor is used as the final storage capacitor (C_{S4}). The transition of the boosting at each stage was observed by monitoring the voltage at the intermediate and the final storage capacitors ($C_{S1}, C_{S2}, C_{S3}, C_{S4}$), which is described using a symbol of voltage meter V_1 – V_4 in this figure.



(a)



(b)

Figure 3. Schematic of the (a) all-pMOS-based CCVM and (b) conventional CMOS-based CCVM with four stages. “P: W/L = 20/0.6 × 10” implies that 10 pMOS transistors with a gate width and length of 20 and 0.6 μm , respectively, are connected in parallel. The N-wells of the transistor, which are surrounded by dashed blue lines, are separated.

A conventional CCVM circuit was also fabricated for comparison of the boosting performance, as shown in Figure 3b. The number of nMOS transistors was gradually increased with the increase in the stages to suppress the degradation of the boosting performance due to the body effect. In this study, the number of transistors in the pMOS-based CCVM in each stage was kept the same because of no body effect problem inherently found in this circuit.

A ring oscillator circuit was also implemented in the IC for generating two-phase clocks to operate these CCVMs, as shown in Figure 4. The output port of the ring oscillator, *OSC out*, and the input port of the buffer circuit, *Buf in*, are separated for characterizing these circuits independently. These are connected in the practical use for generating the two-phase clocks, *CLK_1* and *CLK_2*. The ring oscillator is operated by the power generated from a gastric acid battery and then drives the charge

pumping process. Its duty ratio and period are tuned by tuning the R and C values. Figure 5 shows the photograph of the prototyped IC chip implemented with these circuits. It is clearly seen that the occupied area of the pMOS-based CCVM is half of the conventional CMOS-based CCVM.

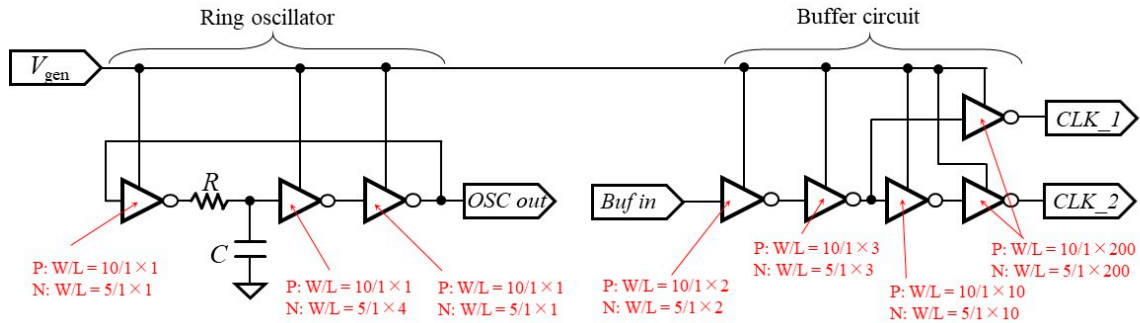


Figure 4. Schematic of the generation circuit of two-phase clocks using a ring oscillator circuit.

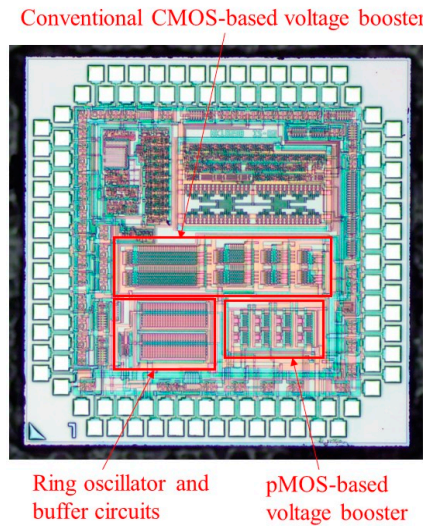


Figure 5. Layout schematic of the prototyped custom IC (0.6 $\mu\text{m}/5$ V CMOS process) for the energy harvesting of the gastric acid power generation.

3. Results and Discussion

3.1. Evaluation of the Voltage-Boosting Performance of the CCVMs

Figure 6 shows the evaluation setup of the voltage-boosting performances of these CCVMs. Here, to characterize the CCVMs independently from the characteristics of the ring oscillator circuit, square wave patterns with 50% duty ratio signals were supplied from a pattern generator to the buffer circuit on the IC. Its high-level voltage was set to the same with V_{gen} as an input voltage. We also simulated the operation behaviors of the CCVMs using LTspice[®] (version IV, Analog Devices, Inc., Norwood, MA, USA).

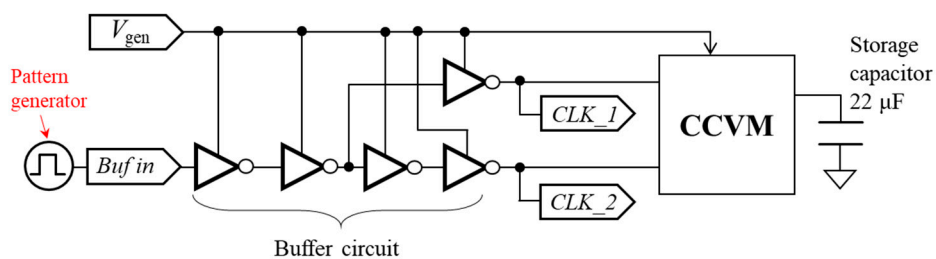


Figure 6. Setup schematic of the characterization of the prototyped CCVMs.

Figure 7 plots the typical simulation result of the voltage-boosting behavior for each CCVM and dependency on the clock frequency when V_{gen} was set as 1.3 V. V_1 of the conventional CMOS-based CCVM is always higher than those of the pMOS-based CCVMs. The boosting performance from V_1 to V_2 is also relatively high. However, the boosting performance worsens gradually as the stages increase owing to the body effect of the nMOS transistors even when the number of nMOS transistors is intentionally increased in the latter stages. The final boosted voltage i.e., V_4 in the conventional CCVM is less than 4 V. By contrast, the ratio of the boosting voltage at each stage is nearly constant and approximately 1.0 V in the pMOS-based CCVMs. Thus, the final boosted voltage, V_4 , reaches 5 V, which is typically higher than that of the conventional CCVM for any clock frequency. In addition, the boosting time shortens as the clock frequency increases.

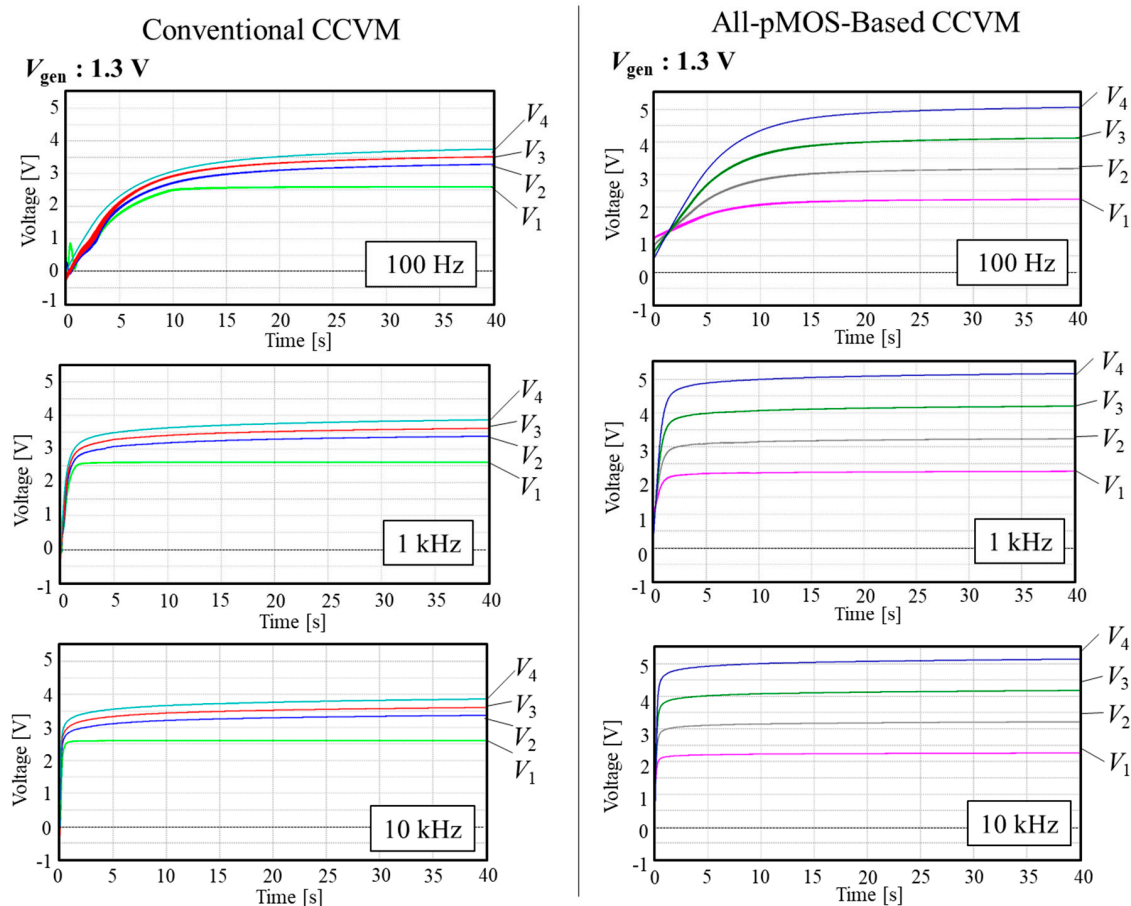


Figure 7. Typical simulation result of the voltage-boosting behavior for each CCVM and dependency on the clock frequency when V_{gen} is set as 1.3 V. V_1 to V_4 correspond to the measured voltage of the intermediate or final storage capacitors at each stage, as shown in Figure 3.

Figure 8 plots the measurement result of the voltage transition for the prototyped circuits. The tendencies are practically the same as those of the simulated result. The voltage-boosting performance is apparently slightly lower than that obtained from the simulation result for the pMOS-based CCVM. Thus, V_4 is also lower than the simulation result value. This may be owing to the mismatch between the actual and assumed characteristics of the transistors.

Figure 9 plots the dependence of the reached voltage of V_4 at 40 s after the boosting process starts, which is symbolized as V_{4_40s} , on V_{gen} (0.85, 1.0, or 1.3 V) and the clock frequency (100 Hz, 300 Hz, 1 kHz, 3 kHz, or 10 kHz). V_{4_40s} increases as V_{gen} increases for both the CCVMs. On the other hand, it is almost independent on the frequency in both the simulation and measurement. The pMOS-based CCVM typically achieves a higher voltage boosting under any condition compare to the conventional CCVM.

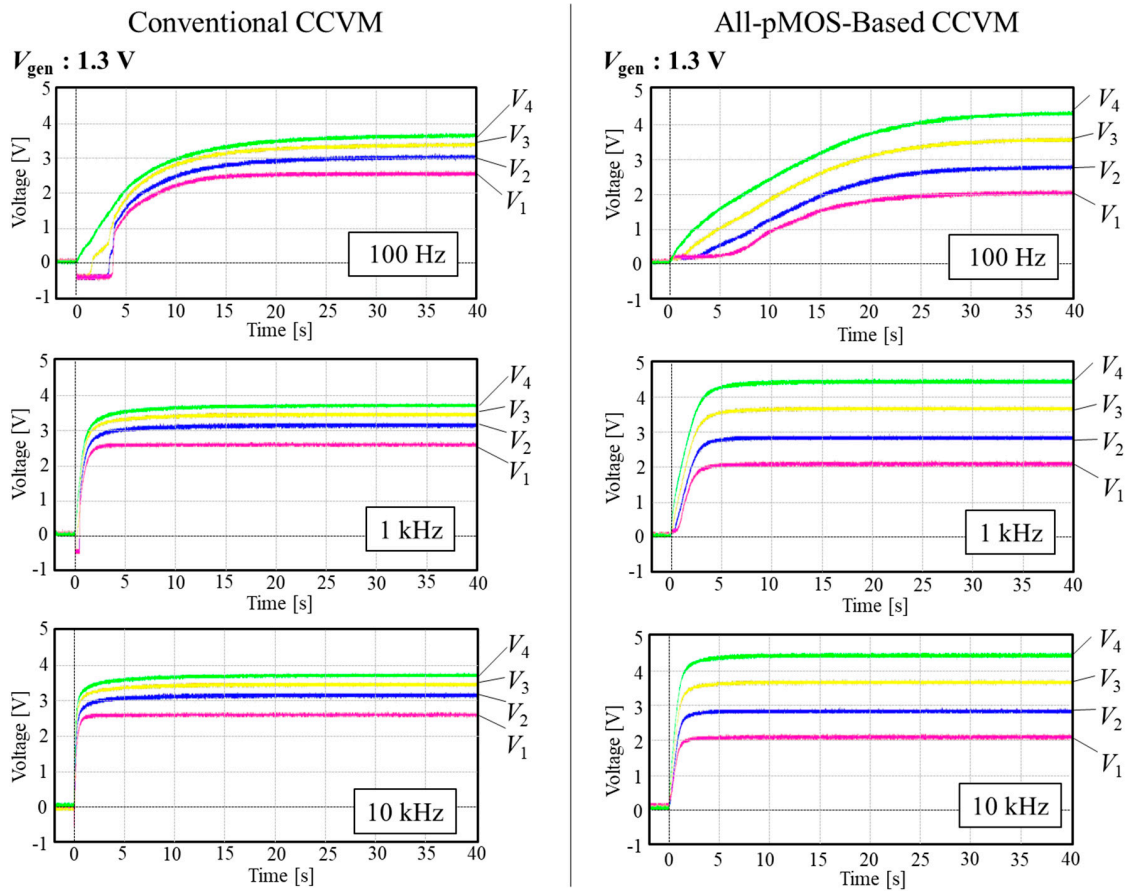


Figure 8. Measurement result of the transition of the boosted voltage at each capacitor in the prototyped circuits.

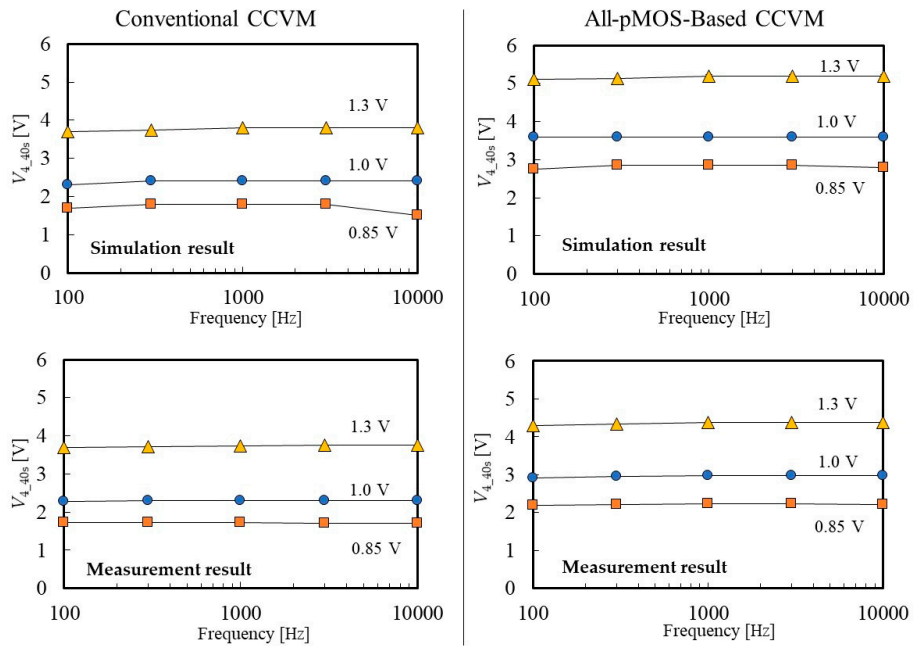


Figure 9. Dependence of the reached voltage (V_{4_40s}) at the fourth stage (V_4) on V_{gen} (0.85, 1.0, or 1.3 V) and clock frequency (100 Hz, 300 Hz, 1 kHz, 3 kHz, or 10 kHz). V_{4_40s} is defined as the V_4 value at 40 s after the boosting process starts.

The dependence of the boosting quickness on V_{gen} and the frequency was also investigated, as plotted in Figure 10. The quickness is defined as the required time until V_4 reaches 63.2% (i.e., $1 - 1/e$) of V_{4_40s} . When V_{gen} is 0.85 V for the measurement results, the required time is significantly longer compared to that under other conditions. This voltage is near the threshold voltage of the transistors. This low V_{gen} probably induced an unperfect switching of transistors and thus resulted in an ineffective boosting process owing to a large leakage current. For both the CCVMs, the times are practically saturated when the frequency is more than 1 kHz. This implies that the amount of the carried charge per unit of time is nearly constant and depends on the conductance of the transistors when the frequency is sufficiently high. The quickness of the pMOS-based CCVM appears to be slower than that of the conventional CMOS-based CCVM with the present circuit constructions. In particular, this is obvious at $V_{\text{gen}} = 0.85$ V. The quickness is improved by optimizing the circuit, such as in terms of the number of pMOS transistors in each stage. Considering that the ionization tendency of Mg is nearly -1.6 V and the previous characterization result of a Mg–Pt battery [13], we can operate the CCVMs at a sufficiently high voltage of more than 1 V. The energy efficiencies of these CCVMs were estimated from simulation to be approximately 15–20% at 1.0–1.3 V as V_{gen} .

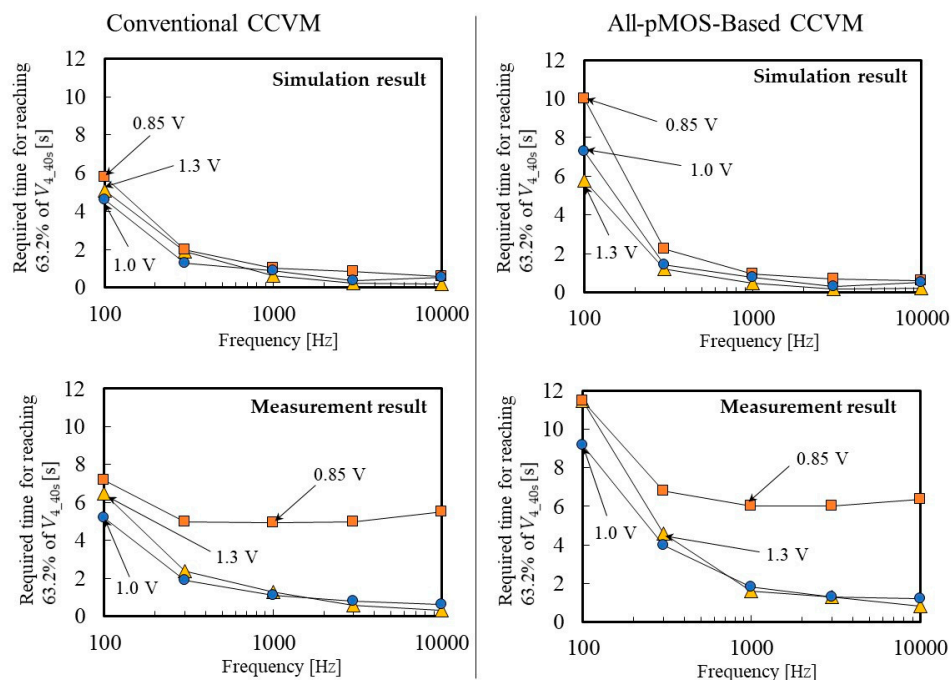


Figure 10. Dependence of the boosting quickness on V_{gen} and the frequency. The quickness is defined as the required time until 63.2% of V_{4_40s} is reached.

3.2. Characterization of the Ring Oscillator Circuit

Next, the dependency of the characteristics of the ring oscillator circuit on the RC values was investigated, as shown in Figure 11. It is clearly seen that the frequency and duty ratio decreased as the supply voltage became lower. Finally, when V_{gen} is below 0.6 V, the oscillation stops. In accordance with the characteristics, the RC combination of 1.2 k Ω /1 nF yields the highest frequency. As mentioned above, this is preferable for rapid boosting. However, the duty ratio is relatively smaller than other RC combinations and will not reach 50% with V_{gen} generated by the Mg–Pt battery. Ideally, it should be approximately 50% for an effective boosting process. In addition, unlike a general button battery, the output voltage of the gastric acid battery in an actual stomach will vary within a certain level because the acid condition will be unstable. Thus, robust parameters for the duty ratio of nearly 50% are preferable for actual use. Therefore, the combination of 120 k Ω /10 nF appears to be best in this study.

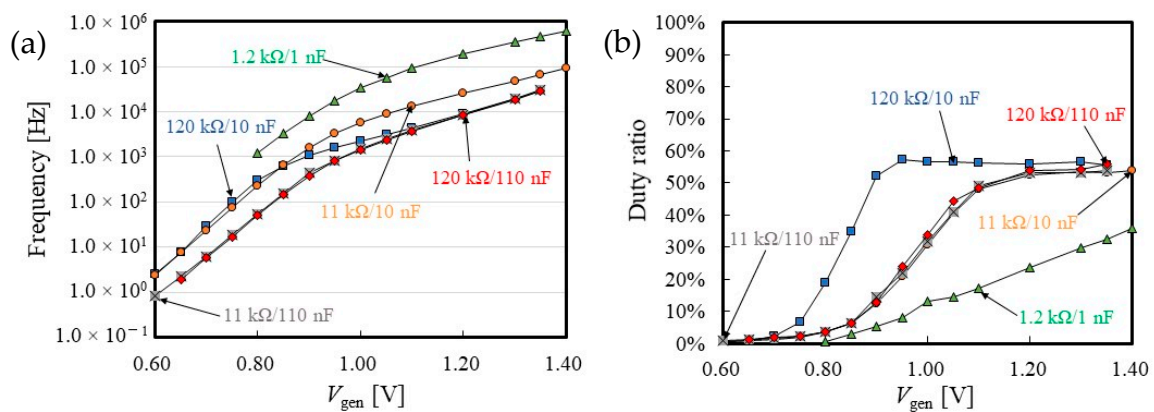


Figure 11. Dependency of (a) the frequency and (b) duty ratio of the ring oscillator circuit on the V_{gen} and RC parameters.

3.3. Demonstration of the Voltage Boosting with the Mg–Pt Gastric Acid Battery and CCVMs

Actual voltage boosting was performed with an artificial gastric acid juice and the CCVMs. A pair of Mg–Pt electrodes with diameters of 2 mm was formed by masking these electrode plates with a water-resistant masking tape, as shown in Figure 12. These electrodes were connected with the energy harvesting domain of the system, as shown in Figure 1. In this experiment, the same capacitors were used for the CCVM as shown in Figure 3. Then, the electrodes were dipped in an artificial gastric juice (pH: ≈ 1.4). The resultant generated power was supplied to the CCVMs and ring oscillator circuit.

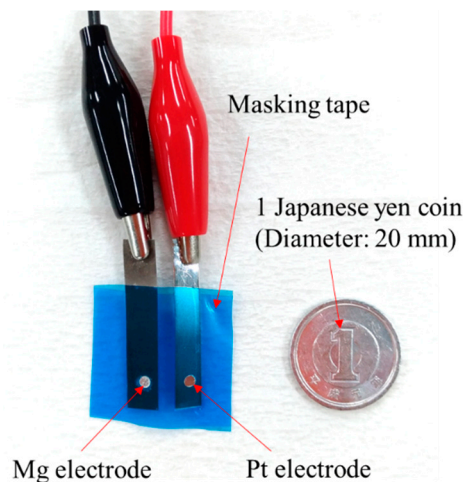


Figure 12. A pair of Mg–Pt electrodes with diameters of 2 mm as a gastric acid battery for the demonstration of energy harvesting via the CCVMs.

In our previous experiment [13], the output power of a pair of Mg–Pt thin films with 6 mm² squares measured 500–1000 μ W in a gastric acid at the output voltage of more than 1 V. Thus, the output power of the electrode in this study was estimated to be 250–500 μ W. Figure 13 shows the boosted voltage transitions. The pMOS-based CCVM achieves a high voltage charge at 5.3 V within 15 s. The frequency and duty ratio of CLK are approximately 70 kHz and 60%, respectively. By contrast, the conventional CMOS-based CCVM provides a lower voltage of 4.8 V in the same manner as for the above-described results.

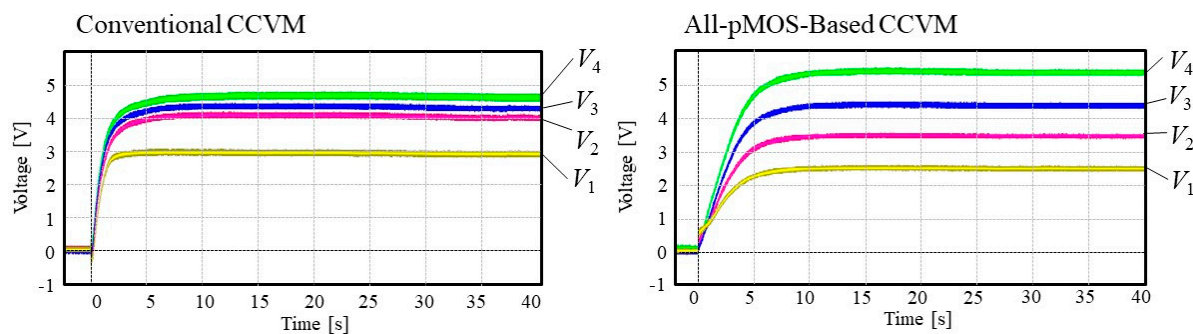


Figure 13. Voltage-boosting behavior at V_1 – V_4 for each CCVM in the Mg–Pt gastric acid battery dipped in an artificial gastric acid juice.

Therefore, we successfully demonstrated that the pMOS-based CCVM based on single-well CMOS technology with two-phase clocks can provide a higher voltage and also a smaller circuit occupied area compared to the conventional CMOS-based CCVM. The saved area on the IC can be implemented with other functional circuits or contribute to miniaturizing the chip size. This CCVM balances well the boosting performance and cost and, thus, will be usable in energy harvesting based on a gastric acid battery. In our previous study, we successfully demonstrated voltage boosting with a conventional CMOS-based CCVM and Mg–Pt gastric acid battery in a dog’s stomach [22]. Therefore, the pMOS-based CCVM promises to demonstrate superior performance.

4. Conclusions

In this study, we prototyped an all-pMOS-based CCVM operated by two-phase clocks with single-well CMOS technology for an energy harvesting application based on a gastric acid battery used in an ingestible device. In the evaluation experiment, the proposed pMOS-based CCVM successfully boosted the input voltage and achieved a higher output voltage than the conventional CMOS-based CCVM under any predetermined condition, due to the elimination of the body effect of the nMOS transistors. In addition, this pMOS-based CCVM was demonstrated to be able to significantly save the occupied footprint on an IC. This is advantageous for implementing other functional circuits on the saved area or reducing the chip size. This superior boosting performance was also confirmed by an experiment using a Mg–Pt gastric acid battery in an artificial gastric juice. We believe that this pMOS-based CCVM with a low-cost standard single-well CMOS process has tremendous potential to become a useful circuit for energy harvesting based on gastric acid power generation.

Author Contributions: S.Y. designed and simulated the voltage-boosting circuits. He also measured the data and wrote the manuscript. H.M. built the setup for the characterizations. T.N. proposed the concept, designed the circuits, contributed to the technical discussions, and reviewed the manuscript.

Funding: This work was supported by JST COI Grant Number JPMJCE1303 and by the Kato Foundation for Promotion of Science.

Acknowledgments: This work was supported by NAITO DENSEI KOGYO CO., LTD.

Conflicts of Interest: The authors declare no conflict of interest.

References

1. Kalantar-Zadeh, K.; Ha, N.; Ou, J.Z.; Berean, K.J. Ingestible sensors. *ACS Sensors* **2017**, *2*, 468–483. [[CrossRef](#)] [[PubMed](#)]
2. Steiger, C.; Abramson, A.; Nadeau, P.; Chandrakasan, A.P.; Langer, R.; Traverso, G. Ingestible electronics for diagnostics and therapy. *Nat. Rev. Mater.* **2019**, *4*, 83–98. [[CrossRef](#)]
3. Bettinger, C.J. Advances in materials and structures for ingestible electromechanical medical devices. *Angew. Chem. Int. Ed.* **2018**, *57*, 16946–16958. [[CrossRef](#)] [[PubMed](#)]

4. Roxane, B.; Chandrou, K.O.; Alexandre, C.P.; Christophe, C.; Bruno, S.; Stéphane, B.; Hervé, N.; Sébastien, M.; Nicolas, B. Gastrointestinal thermal homogeneity and effect of cold water ingestion. *J. Therm. Biol.* **2018**, *78*, 204–208. [[CrossRef](#)] [[PubMed](#)]
5. Hoffmann, M.E.; Rodriguez, S.M.; Zeiss, D.M.; Wachsberg, K.N.; Kushner, R.F.; Landsberg, L.; Linsenmeier, R.A. 24-h core temperature in obese and lean men and women. *Obesity* **2012**, *20*, 1585–1590. [[CrossRef](#)] [[PubMed](#)]
6. Koziolok, M.; Grimm, M.; Becker, D.; Iordanov, V.; Zou, H.; Shimizu, J.; Wanke, C.; Garbacz, G.; Weitschies, W. Investigation of pH and temperature profiles in the GI tract of fasted human subjects using the Intellicap[®] system. *J. Pharm. Sci.* **2015**, *104*, 2855–2863. [[CrossRef](#)] [[PubMed](#)]
7. Kalantar-Zadeh, K.; Berean, K.J.; Ha, N.; Chrimes, A.F.; Xu, K.; Grando, D.; Ou, J.Z.; Pillai, N.; Campbell, J.L.; Brkljača, R.; et al. A human pilot trial of ingestible electronic capsules capable of sensing different gases in the gut. *Nat. Electron.* **2018**, *1*, 79–87.
8. Bongers, C.C.W.G.; Hopman, M.T.E.; Eijsvogels, T.M.H. Validity and reliability of the myTemp ingestible temperature capsule. *J. Sci. Med. Sport* **2018**, *21*, 322–326. [[CrossRef](#)] [[PubMed](#)]
9. Nadeau, P.; El-Damak, D.; Glettig, D.; Kong, Y.L.; Mo, S.; Cleveland, C.; Booth, L.; Roxhed, N.; Langer, R.; Chandrakasan, A.P.; et al. Prolonged energy harvesting for ingestible devices. *Nat. Biomed. Eng.* **2017**, *1*, 0022. [[CrossRef](#)] [[PubMed](#)]
10. Hafezi, H.; Robertson, T.L.; Moon, G.D.; Au-Yeung, K.Y.; Zdeblick, M.J.; Savage, G.M. An ingestible sensor for measuring medication adherence. *IEEE Trans. Biomed. Eng.* **2015**, *62*, 99–109.
11. Flores, G.P.; Carnes, T.C.; Baumgartner, S.L.; Buffkin, D.E.; Euliano, N.R.; Smith, L.N. Performance, reliability, usability, and safety of the id-cap system for ingestion event monitoring in healthy volunteers: A pilot study. *Innov. Clin. Neurosci.* **2016**, *13*, 12–19. [[PubMed](#)]
12. Yoshida, S.; Miyaguchi, H.; Nakamura, T. Development of tablet-shaped ingestible core-body thermometer powered by gastric acid battery. *IEEE Sens. J.* **2018**, *18*, 9755–9762.
13. Yoshida, S.; Miyaguchi, H.; Nakamura, T. Concept proof of low-energy consumption and compact ingestible thermometer based on gastric acid power generation. *IEEJ Trans. Sensors Micromach.* **2018**, *138*, 164–169. [[CrossRef](#)]
14. Peng, H.; Tang, N.; Yang, Y.; Heo, D. CMOS startup charge pump with body bias and backward control for energy harvesting step-up converters. *IEEE Trans. Circuits Syst. I Regul. Pap.* **2014**, *61*, 1618–1628. [[CrossRef](#)]
15. Pelliconi, R.; Iezzi, D.; Baroni, A.; Pasotti, M.; Rolandi, P.L. Power efficient charge pump in deep submicron standard CMOS technology. *IEEE J. Solid-State Circuits* **2003**, *38*, 1068–1071. [[CrossRef](#)]
16. Yan, N.; Min, H. High efficiency all-PMOS charge pump for low-voltage operations. *Electron. Lett.* **2006**, *42*, 277–279.
17. Li, N.; Huang, Z.; Jiang, M.; Inoue, Y. High efficiency four-phase all PMOS charge pump without body effects. In Proceedings of the 2008 International Conference on Communication Circuits Systems, Xiamen, China, 25–27 May 2008; pp. 1083–1087.
18. Liu, J.; Bazzini, A.; Gregori, S. Fully-integrated PMOS-based charge pumps in standard CMOS process without high-voltage switches. In Proceedings of the 2012 25th IEEE Canadian Conference on Electrical and Computer Engineering (CCECE), Montreal, QC, Canada, 29 April–2 May 2012; pp. 1–4.
19. Lee, J.C.; Chung, Y. PMOS-switching dual-path charge pump in standard twin-well CMOS technology. *Int. J. Electron.* **2010**, *97*, 273–283. [[CrossRef](#)]
20. Lauterbach, C.; Weber, W.; Römer, D. Charge sharing concept and new clocking scheme for power efficiency and electromagnetic emission improvement of boosted charge pumps. *IEEE J. Solid-State Circuits* **2000**, *35*, 719–723. [[CrossRef](#)]
21. Jiang, X.; Yu, X.; Moez, K.; Elliott, D.G.; Chen, J. High-efficiency charge pumps for low-power on-chip applications. *IEEE Trans. Circuits Syst. I Regul. Pap.* **2018**, *65*, 1143–1153. [[CrossRef](#)]
22. Yoshida, S.; Miyaguchi, H.; Nakamura, T. Proof of Concept for Tablet-Shaped Ingestible Core-Body Thermometer with Gastric Acid Battery. In Proceedings of the 2019 IEEE 1st Global Conference on Life Sciences and Technologies (LifeTech 2019), Osaka, Japan, 12–14 March 2019; pp. 182–184.

